Design and Optimization of Pressurized Toroidal LPG Fuel Tanks with Variable Section

Assoc. Prof. PhD. Eng. **Mihai ŢĂLU**[1], Assoc. Prof. PhD. Eng. **Ștefan ŢĂLU**[2,*]

[1] University of Craiova, Faculty of Mechanics, Department of Applied Mechanics and Civil Engineering, Calea București Street, no. 107, 200512 Craiova, Dolj county, Romania. E-mail: mihai_talu@yahoo.com

[2] Technical University of Cluj-Napoca, The Directorate of Research, Development and Innovation Management (DMCDI), Constantin Daicoviciu Street, no. 15, Cluj-Napoca, 400020, Cluj county, Romania. Corresponding author* e-mail: stefan_ta@yahoo.com

Abstract: *This study addresses the design and optimization of the pressurized toroidal LPG fuel tanks with variable section used in automotive industry based on the finite element analysis (FEA) approaches, to model both thermal and mechanical processing conditions. To define specific key performance indicators and to determine the optimal form of toroidal LPG fuel tank with the minimum stress state and linear deformation was applied a mathematical and mechanical foundation for the design and optimization. Computer aided investigations are carried out using 3D models done in the AutoCAD Autodesk 2017 software, which were imported to SolidWorks 2017 software for analysis and can offer an important reference for the design of toroidal LPG fuel tanks.*

Keywords: *Automotive industry, industrial engineering design, optimization methods, pressurized toroidal LPG fuel tank*

1. Introduction

During the past decades, the computer aided engineering design methods to produce pressurized fuel tanks in the automotive industry [1-3] have been developed in a variety of directions to improve vehicle's performance [4-6]. The storage fuel tanks, made from aluminum alloys or various types of steel, are used in the automotive industry for safely storing fuel: compressed natural gas (CNG) or liquefied petroleum gas (LPG) [7-12]. The design, construction, installation, testing and monitoring requirements of the storage fuel tanks (to maintain structural integrity at high pressures) are bounded and regulated by various codes and standards [13-15].

The design procedure of the fuel tanks involves various assumptions, supershapes design variables [16, 17], specific structure parameters [14], design constraints [15], computer tools [18-23], numerical computational methods [24-26], CAD visualization techniques [27-34], test data and experimental data, that permit to obtain an optimal product with a low structural weight and a high structural performance.

The pressurized toroidal LPG fuel tanks have been recognized as a volumetrically efficient storage solution that can reduce final product mass, while improving storage efficiencies [14, 15].

In our study, a finite element analysis of pressurized toroidal LPG fuel tank to meet safety standards and optimization was conducted considering specific geometry and structure parameters.

2. Design methodology

In our study, optimal design of toroidal cross-sectional profiles (considering shape and thickness variation) in order to reduce stress non-uniformity is performed.

2.1 Basic geometry of toroidal surfaces

Let's consider the surface generated by revolving of a closed generating curve C_G along a guiding curve C_{D1}, being tangent in the movement on a second internal curve C_{D2}, as shown in fig. 1a.

The curve C_G (that generates the cross-section) is located in a vertical plane, whereas the reference curves C_{D1} and C_{D2} (that determine the variation in the cross-sectional dimensions) are coplanar and situated in the horizontal plane.

An example of the manufactured product with the apparature monted on the tank that permit an easy access to the filling or drainage connections of fuel tank is shown in fig. 1c.

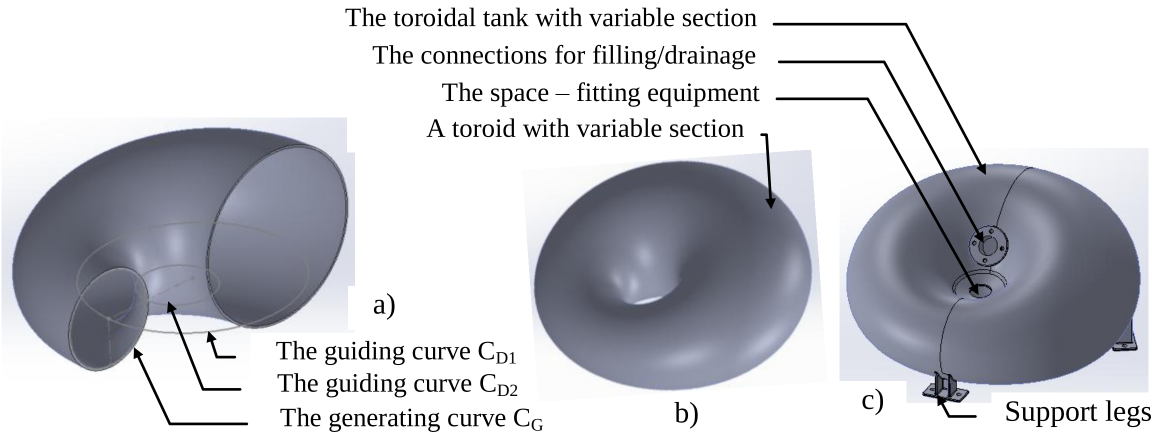

Fig. 1. a) The ½ section of a toroidal tank; b) The model of a toroidal tank; c) The tank constructive solution

The graphical representations of toroidal symmetrical parts in respect with the symmetrical planes is shown in orthogonal views in fig. 2a and 2b, while the axonometric representation is shown in fig. 2c.

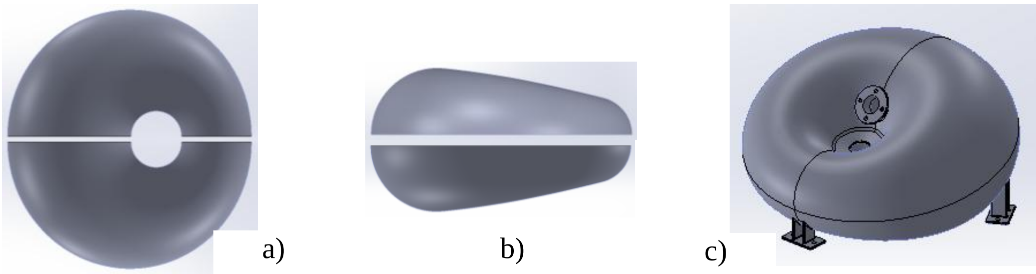

Fig. 2. a) and b) The orthogonal views with the symmetry horizontal plane; c) The axonometric representation of the tank constructive solution

The generating curves and the directories curves are closed curves that do not intersect on themselves, such as: ellipses, circles, triangles, rectangles, etc. Some graphical examples of toroids with variable section are shown in figs. 3 and 4.

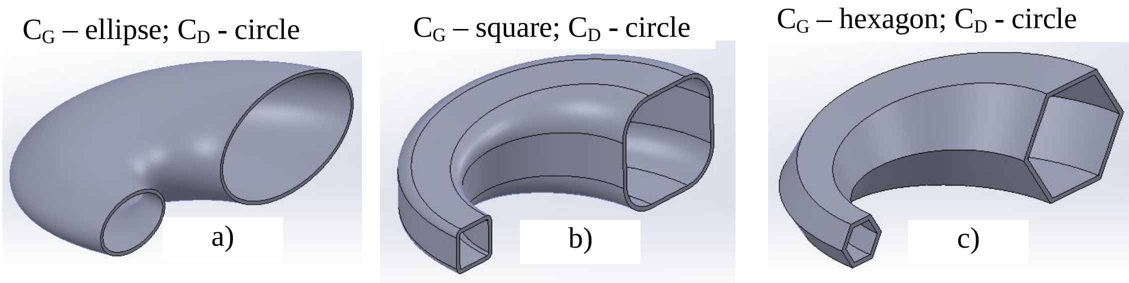

Fig. 3. The axonometric representation of a ½ toroid sectioned generated by: a) C_G – ellipse and C_D – circle; b) C_G – square and C_D – circle; c) C_G – hexagon and C_D – circle

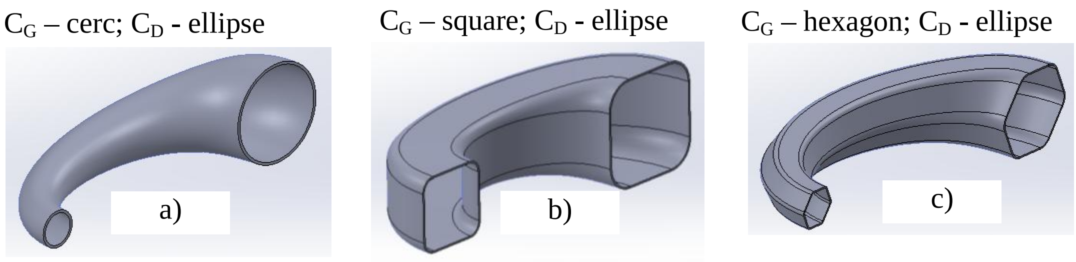

Fig. 4. The axonometric representation of a ½ toroid sectioned generated by: a) C_G – circle and C_D – ellipse; b) C_G – square and C_D – ellipse; c) C_G – hexagon and C_D - ellipse

2.2 The geometrical model selected for numerical analysis

The geometrical model selected for numerical analysis is shown in fig. 5a (C_G – ellipse and C_D – circle), with next numerical values for the diameters of circles: C_{D1} and C_{D2} (C_{D1} = 300 mm and C_{D1} = 130 mm). The eccentricity of the curves: C_{D1} and C_{D2} has the value of e = 25 mm.
The axonometric isometric view of the parameterized geometrical model (non-sectioned and sectioned to ¾ and ½ of the initial model, as a consequence of the tank constructive symmetry) is shown in fig. 5.

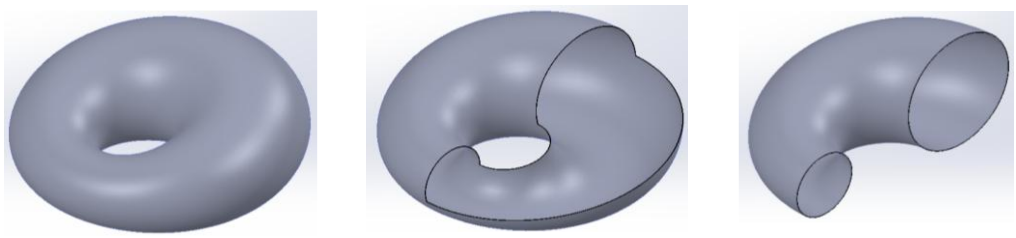

a) b) c)

Fig. 5. The geometrical model: a) non-sectioned; b) sectioned at ¾; c) sectioned at ½

The modeling was done in the AutoCAD Autodesk 2017 software [35] and the optimization analysis to ensure quality, performance, and safety was performed with SolidWorks 2017 software [36] with the: Static, Thermal and Design Study modules.
The specified surfaces to which the constraints and restrictions are applied are shown in fig. 6.

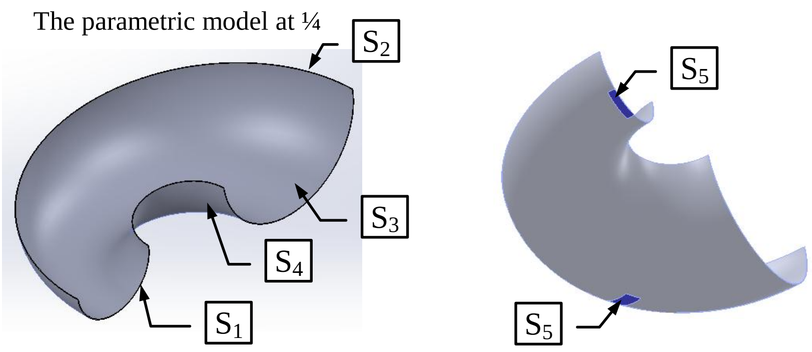

a) b)

Fig. 6. The geometrical model at ¼ with the specified surfaces

The design data used in this analysis are:
- the maximum static hydraulic pressure: p_{max} = 3 N/mm^2 applied to the surface S_3;
- the working temperature between the limits: T = -30 ^{0}C to T = 60 ^{0}C applied to the surface S_4;
- the symmetry on surfaces: S_1 and S_2;
- the fixed surfaces located on the legs support on S_5 (shown in Fig. 5b);
- the execution material for tank is AISI 4340 laminated steel;
- the exploitation time of tank is: n_a = 20 years;
- the corrosion velocity of material: v_c = 0.09 mm/year.

The optimal design issue here refers to the non-linear constrained optimization and involves minimizing the structural weight W (associated with the cover thickness s = 0.5...3 mm), subjected to the non-linear design constraints (the maximum Von Mises stress must by less than or equal to the admissible traction value of the material, $\sigma_{rez} \leq \sigma_a = 710\ N/mm^2$).
Applying the numerical optimization procedure for T = -30 ^{0}C, the following values were obtained: thickness s = 0.9 mm; the maximum Von Mises stress $\sigma_{rez.\ max}$= 703.073 N/mm^2 and the linear deformation u_{max} = 0.533 mm.
The graphs of Von Mises stress and linear deformation distribution computed for T = -30 ^{0}C are shown in fig. 7.

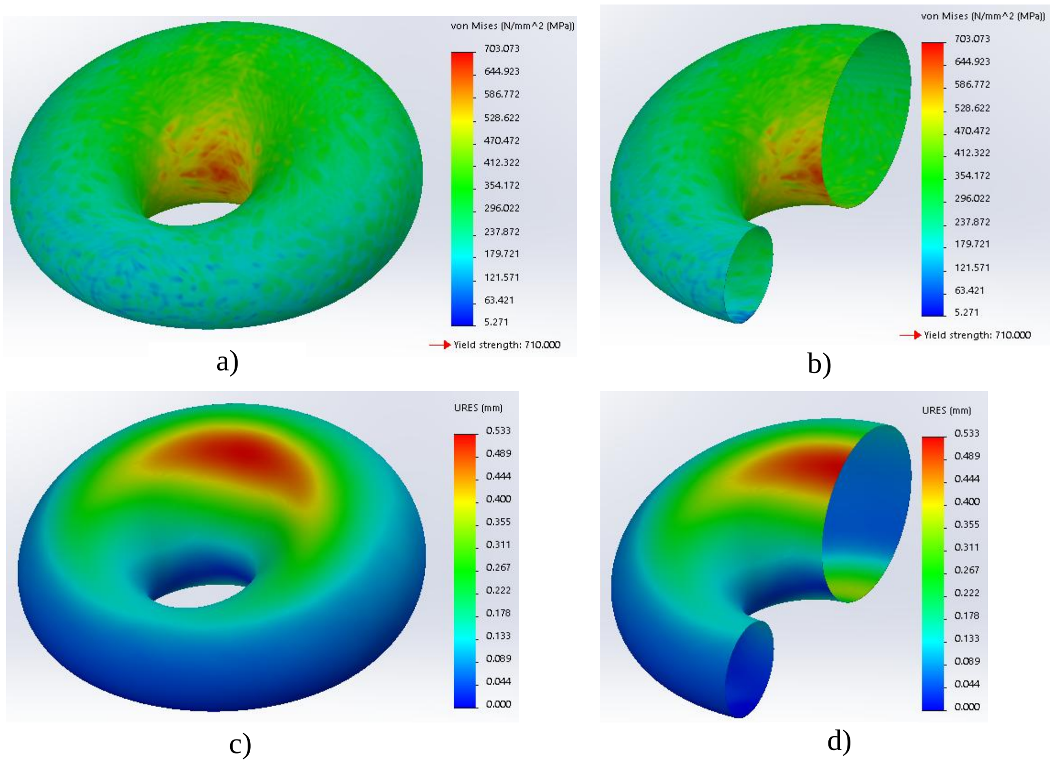

Fig. 7. The graphs of: I) Von Mises stress distribution: a) non-sectioned model and b) sectioned model; II) linear deformation distribution: c) non-sectioned model and d) sectioned model

The optimal thickness is corrected considering the influence of the corrosion phenomenon and the negative tolerance of the metal sheet, using the following formula [10]:

$$s_{real} = s_{opt} + \Delta s_c + \Delta s_T + \Delta s_{am} = s_{opt} + v_c \cdot n_a + abs(A_i) + 0.1 \cdot s \quad (1)$$

where:
- Δs_c, the additional thickness used to compensate the loss of thickness due to the corrosion process;
- Δs_T, the additional thickness used to compensate the loss due to the negative tolerance of the execution of laminate metal sheet;
- v_c, the corrosion velocity of the metal sheet, v_c = 0.08 mm/year;
- n_a, the number of years of exploitation, n_a = 20 years;
- A_i, the negative tolerance of the laminate sheet, A_i = - 0.6 mm;
- Δs_{am} = 0.1·s, the additional thickness used to compensate the thinning of wall into the embossing process, Δs_{am} = 0.4 mm.

By substituting the numerical values, the minimum thickness of the laminate sheet has the following value:

$$s_{real\ min} = 0.9 + 0.09 \cdot 20 + abs(-0.6) + 0.1 \cdot 4 = 3.7\ mm \quad (2)$$

For the execution, we choose a laminate sheet of AISI 4340 steel that has a thickness of $s = 4^{+0.25}_{-0.6}$ mm.

2.3 Three-dimensional stress and strain analysis

In these analyses, the following hypothesis has been applied for the formulation of stresses and strains: a) the 3-D model is subjected to axisymmetric loading and keeps symmetry before and after deformation.
For n_a = 0 years and temperature T = -30 ^{0}C, the numerical value of pressure p = 13.68 N/mm^2 and the corresponding graphs of Von Mises stress distribution and linear deformation distribution are shown in fig. 8.

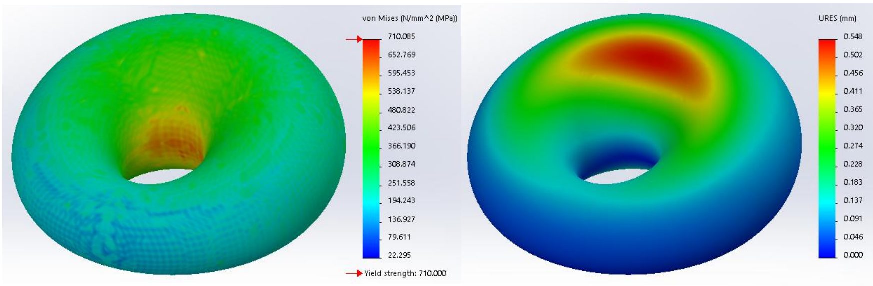

a) b)

Fig. 8. The graphs of: a) Von Mises stress distribution; b) linear deformation distribution; both computed for p_{max}, T = -30 ^{0}C and n_a = 0 years.

The graphs of Von Mises stress distribution and linear deformation distribution (computed for explosion pressure, T = -30 ^{0}C) were shown on the sectioned model at ½ in figures 9b and 9d and in figures 9a and 9c for the entire model. For n_a = 0 years and T = -30 ^{0}C, the computed tank explosion pressure is p = 21.65 N/mm^2 and the maximum linear deformation is u_{max} = 0.855 mm.

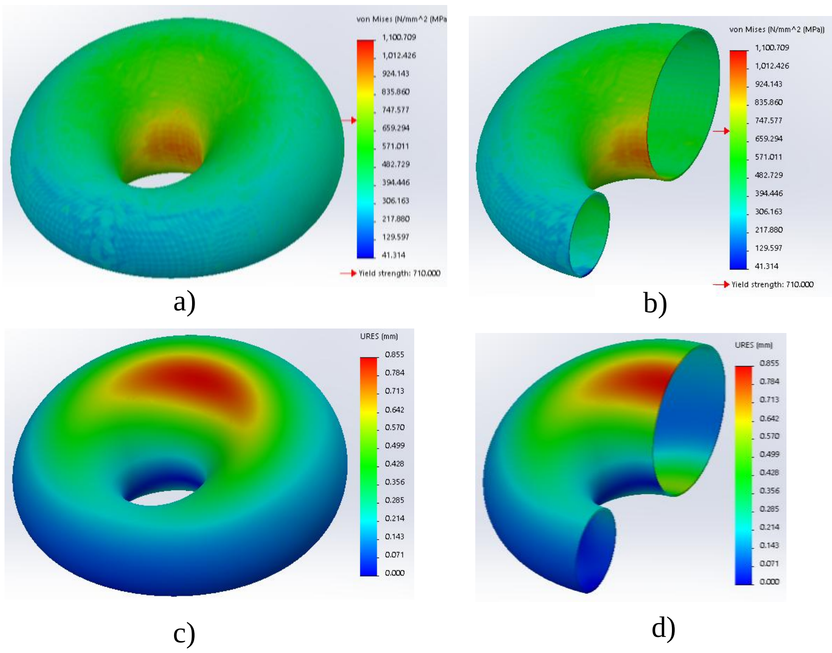

Fig. 9. The graphs of: I) Von Mises stress distribution: a) non-sectioned model and b) sectioned model; II) linear deformation distribution: c) non-sectioned model and d) sectioned model; both computed for the explosion pressure and T = -30 ^{0}C.

It can be revealed that the explosion pressure is greater by 7.21 times than the maximum test pressure of the fuel tank.
The numerical values of state of stress and linear deformation distribution are given in Table 1.

Table 1: The Von Mises stress and linear deformation of geometrical model

			T [^{0}C]									
No. of years		**s[mm]**	-30 ^{0}C	-20 ^{0}C	-10 ^{0}C	0 ^{0}C	10 ^{0}C	20 ^{0}C	30 ^{0}C	40 ^{0}C	50 ^{0}C	60 ^{0}C
0	σ[MPa]	4	212.57	191.01	174.58	163.27	159.04	156.03	160.08	169.27	183.57	202.99
	u[mm]		0.1073	0.1112	0.1156	0.1204	0.1255	0.1314	0.1376	0.1442	0.1512	0.1587
5	σ[MPa]	3.55	231.19	211.49	194.74	183.86	174.43	168.09	169.58	174.13	193.49	213.83
	u[mm]		0.123	0.127	0.132	0.137	0.143	0.150	0.156	0.163	0.170	0.178
10	σ[MPa]	3.1	235.66	226.12	216.87	207.92	199.31	191.09	192.23	195.78	212.18	233.91
	u[mm]		0.145	0.149	0.154	0.160	0.166	0.172	0.179	0.186	0.193	0.200
15	σ[MPa]	2.65	282.65	264.64	252.84	241.91	231.33	221.67	221.92	234.47	256.54	279.47
	u[mm]		0.177	0.182	0.187	0.192	0.199	0.205	0.211	0.218	0.225	0.232
20	σ[MPa]	1.2	550.48	532.83	515.58	498.78	483.92	478.44	494.58	511.66	529.59	548.27
	u[mm]		0.406	0.412	0.417	0.423	0.429	0.435	0.441	0.447	0.454	0.46
Opti-mal	σ[MPa]	0.9	703.07	685.97	669.18	652.70	636.57	620.82	616.51	636.32	656.87	677.48
	u[mm]		0.533	0.538	0.544	0.549	0.555	0.560	0.566	0.571	0.577	0.583

The graphical representations of Von Mises stress σ(s, T) and the linear deformation, u(s, T) as specified in Table 1, are shown in figures 10 and 11.

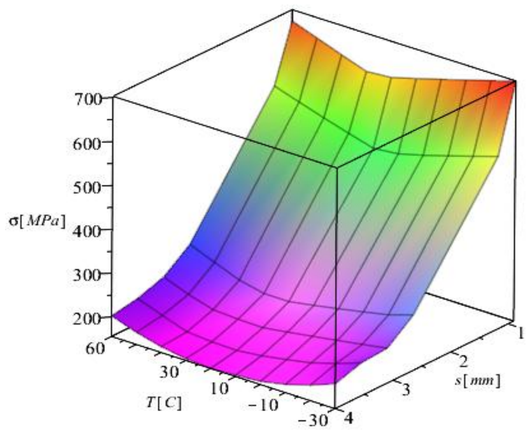

Fig. 10. The graph of Von Mises stress σ(s, T)

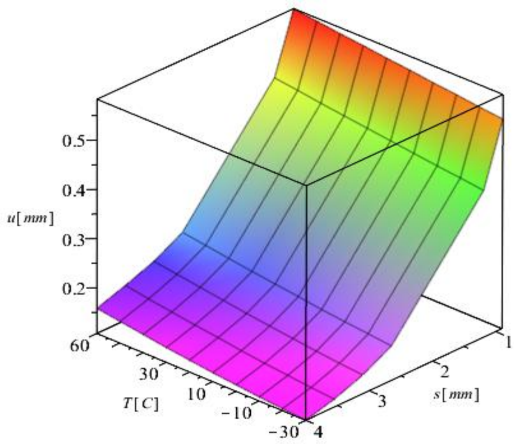

Fig. 11. The graph of linear deformation u(s, T)

The graphs of Von Mises stress (for n_a = 0 years and n_a = 20 years) is shown in fig. 12 and 13 with the corresponding the laws of stress variation computed by polynomial interpolation.

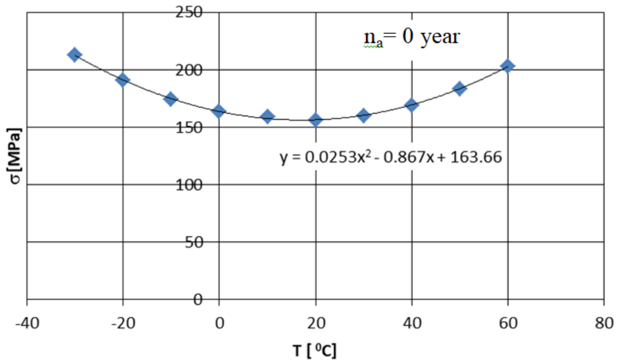

Fig. 12. The graph of Von Mises stress at n_a = 0 years

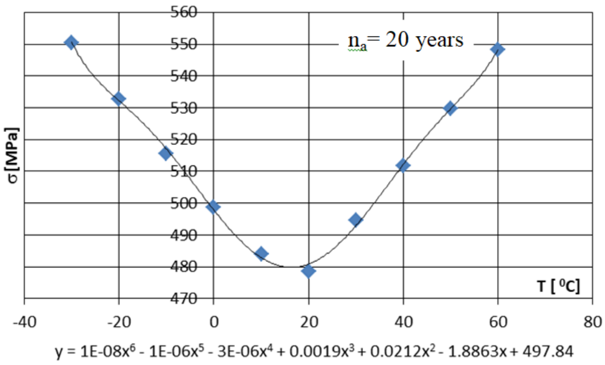

Fig. 13. The graph of Von Mises stress at n_a = 20 years

The laws of stress variation computed by polynomial interpolation are given in Table 2.

Table 2: The laws of stress variation computed by polynomial interpolation

n_a [years]	s[mm]	$\sigma(t)$ [MPa]
0	4	$\sigma(t)=0.0253\cdot T^2-0.867\cdot T+163.88$
5	3.55	$\sigma(t)=2\cdot10^{-7}\cdot T^5+6\cdot10^{-6}\cdot T^4-0.0003\cdot T^3+0.0153\cdot T^2-0.9889\cdot T+183.27$
10	3.1	$\sigma(t)=-2\cdot10^{-8}\cdot T^5+6\cdot10^{-6}\cdot T^4+0.0002\cdot T^3+0.0013\cdot T^2-0.9278\cdot T+207.79$
15	2.65	$\sigma(t)=-2\cdot10^{-7}\cdot T^5+2\cdot10^{-5}\cdot T^4+0.0003\cdot T^3-0.0038\cdot T^2-1.1523\cdot T+242.06$
20	1.2	$\sigma(t)=-1\cdot10^{-6}\cdot T^5-3\cdot10^{-6}\cdot T^4+0.0019\cdot T^3+0.0212\cdot T^2-1.8863\cdot T+497.84$

The graphs of linear deformations (for n_a = 0 years and n_a = 20 years) is shown in fig. 14 and 15 with the corresponding the laws of linear deformations variation computed by polynomial interpolation.

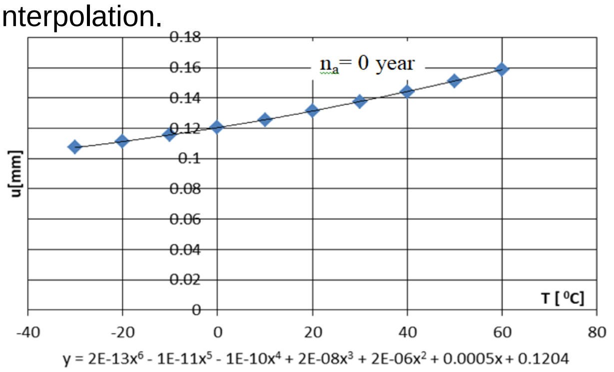

Fig. 14. The graph of linear deformations at n_a = 0 years

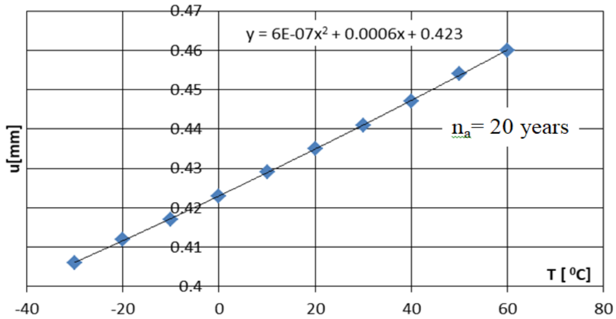

Fig. 15. The graph of linear deformations at n_a = 20 years

The laws of linear deformations variation computed by polynomial interpolation are given in Table 3.

Table 3: The laws of linear deformations variation computed by polynomial interpolation

n_a [years]	s [mm]	$\sigma(t)$ [MPa]
0	4	$\sigma(t)=-1\cdot10^{-11}\cdot T^5-1\cdot10^{-10}\cdot T^4+2\cdot10^{-8}\cdot T^3+2\cdot10^{-6}\cdot T^2+0.0005\cdot T+0.1204$
5	3.55	$\sigma(t)=1\cdot10^{-11}\cdot T^5+6\cdot10^{-4}\cdot T^4-3\cdot10^{-8}\cdot T^3+3\cdot10^{-6}\cdot T^2-0.0006\cdot T+0.1371$
10	3.1	$\sigma(t)=-3\cdot10^{-11}\cdot T^5+1\cdot10^{-9}\cdot T^4+5\cdot10^{-9}\cdot T^3+1\cdot10^{-6}\cdot T^2+0.0006\cdot T+0.1599$
15	2.65	$\sigma(t)=9\cdot10^{-11}\cdot T^5-6\cdot10^{-10}\cdot T^4-1\cdot10^{-7}\cdot T^3+3\cdot10^{-6}\cdot T^2+0.0006\cdot T+0.1924$
20	1.2	$\sigma(t)=6\cdot10^{-7}\cdot T^2+0.0006\cdot T+0.423$

The graphs of Von Mises stress computed for T = -30 ^{0}C for: a) the geometrical model (Fig. 16a); b) and c) on the outer and the inner circumference of geometrical model (fig. 16b and 16c).

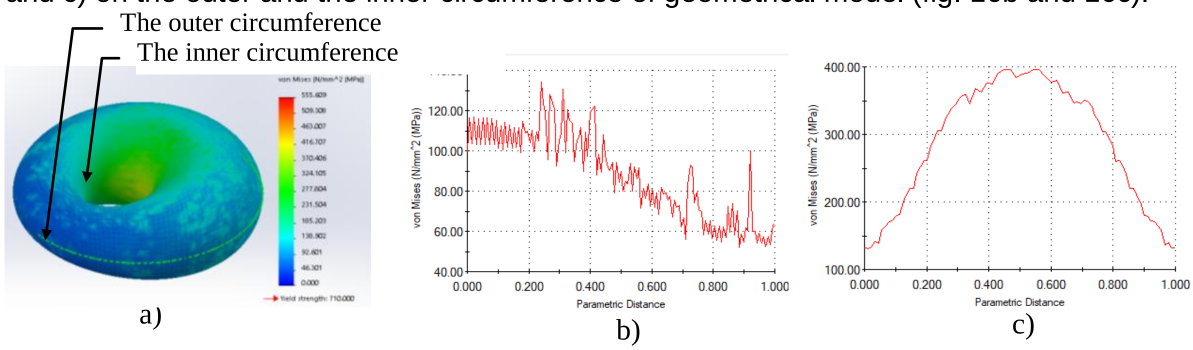

Fig. 16. The graphs of Von Mises stress computed for T = -30 ^{0}C for: a) the geometrical model; b) and c) on the outer and on the inner circumference of geometrical model

The graphs of linear deformations computed for T = 60 ^{0}C for: a) the geometrical model (fig. 17a); b) and c) on the outer and the inner circumference of geometrical model (fig. 17b and 17c).

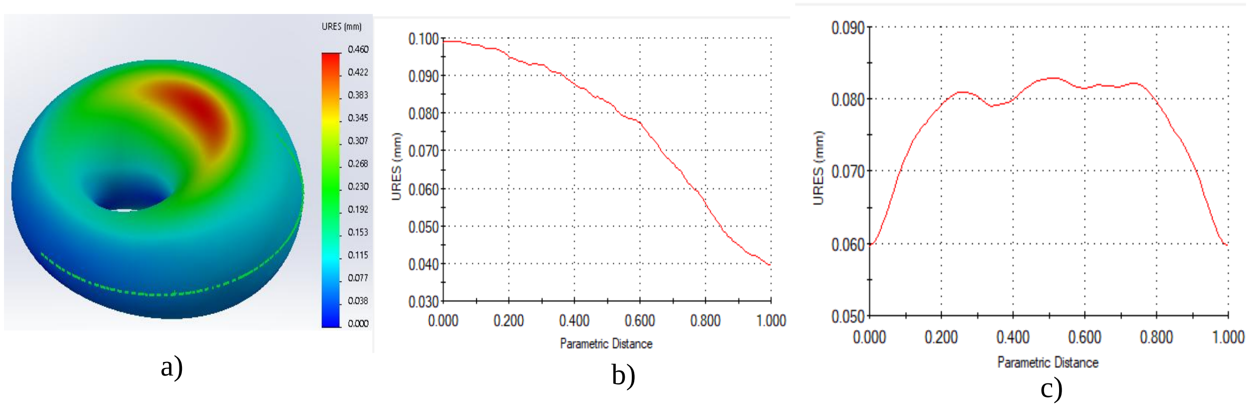

Fig. 17. The graphs of linear deformations computed for T = 60 ^{0}C for: a) the geometrical model; b) and c) on the outer and the inner circumference of geometrical model

The graphs of Von Mises stress computed for T = -30 ^{0}C for: a) the geometrical model (fig. 18a); b) and c) on the minimum circumference of circle and on the maximum circumference of circle (fig. 18b and 18c).

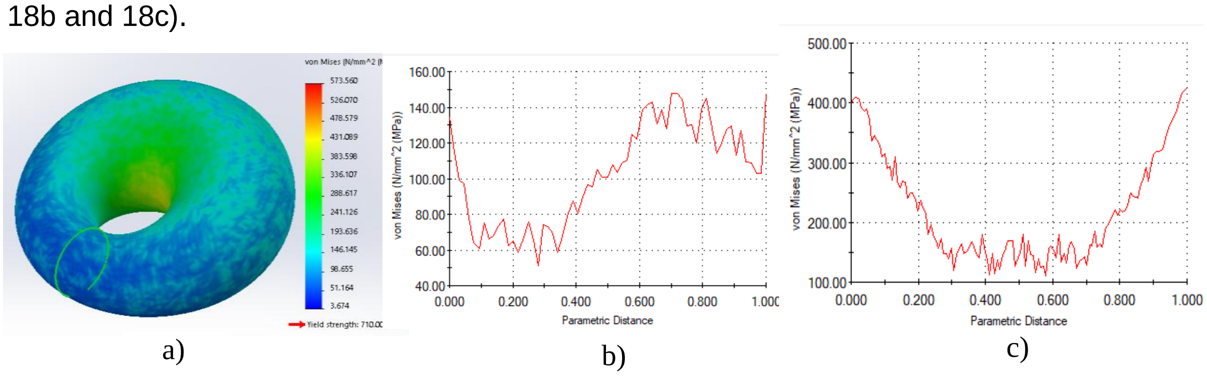

Fig. 18. The graphs of Von Mises stress computed for T = -30 ^{0}C for: a) the geometrical model; b) and c) on the minimum circumference of circle and on the maximum circumference of circle

The graphs of linear deformations computed for T = 60 ^{0}C for: a) the geometrical model (fig. 19a); b) and c) on the minimum circumference of circle and on the maximum circumference of circle (fig. 19b and 19c).

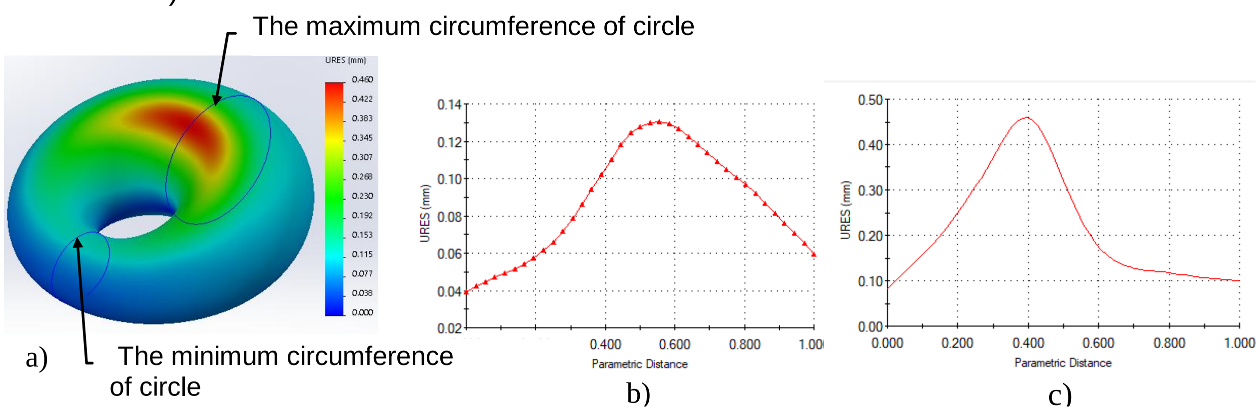

Fig. 19. The graphs of linear deformations computed for T = 60 ^{0}C for: a) the geometrical model; b) and c) on the minimum circumference of circle and on the maximum circumference of circle

3. Discussion

The maximum value of the Von Mises stress (σ = 703.07 MPa) occurs at T = - 30 ^{0}C, while the maximum linear deformation (u_{max} = 0.583 mm) occurs at T = 60 ^{0}C, (as shown in Table 1).

The maximum working pressure at T = -30 ^{0}C is 4.56 times higher than the hydraulic test pressure and the explosion pressure is 1.583 times higher than the maximum working pressure. In the case of linear deformations associated with these two pressures their ratio is u_r / u_{max} = 1.604.
It was revealed that the Von Mises stress and the linear deformations increase simultaneously with the increase of the temperature and the exploitation period, (as shown in fig. 9 and 10).
For n_a = 0 years, the Von Mises stress shows a minimum of σ = 156.03 MPa (at temperature T = 20 ^{0}C), and for n_a = 20 years a minimum of σ = 483.92 MPa (at temperature T = 10 ^{0}C), (as shown in Table 1).

4. Conclusions

In this study, an elaboration of the design and optimization procedure associated with the pressurized toroidal LPG fuel tanks with variable section used in automotive industry based on the FEA approaches were performed. Computer aided investigations were employed to predict the mechanical behavior of toroidal LPG fuel tanks, corresponding to various design scenarios, in order to improve the structural performance for a feasible solution within a prescribed tolerance.
A new possibility to improve the pressurized toroidal LPG fuel tanks performance can be offered by the application of adapted cross-sectional shapes instead of the conventional shapes.
The results revealed that the optimal toroidal geometry provides a lower weight and lower aspect ratio than the circular one, and thus leads to better structural performance and an alternative to spaces having limited height and volume. Determination of the optimal geometric toroidal model with the minimum number of appropriate design variables through the combination of equations and the optimality conditions would also be considered as design objectives in the future study.

Financial disclosure: Neither author has a financial or proprietary interest in any material or method mentioned.
Competing interests: The authors declare that they have no significant competing financial, professional or personal interests that might have influenced the performance or presentation of the work described in this manuscript.

References

[1] Ghiţă, C. Mirela, Anton C. Micu, Mihai Ţălu, Ştefan Ţălu and Ema I. Adam. "Computer-Aided Design of a classical cylinder gas tank for the automotive industry." *Annals of Faculty of Engineering Hunedoara - International Journal of Engineering, Hunedoara*, *Romania*, Tome XI, Fascicule 4 (2013): 59-64.
[2] Ghiţă, C. Mirela, Anton C. Micu, Mihai Ţălu and Ştefan Ţălu. "Shape optimization of vehicle's methane gas tank." *Annals of Faculty of Engineering Hunedoara - International Journal of Engineering, Hunedoara, Romania*, Tome X, Fascicule 3 (2012): 259-266.
[3] Ghiţă, C. Mirela, Ştefan C. Ghiță, Ştefan Ţălu and Simona Rotaru, "Optimal design of cylindrical rings used for the shrinkage of vehicle tanks for compressed natural gas." *Annals of Faculty of Engineering Hunedoara - International Journal of Engineering, Hunedoara*, Tome XII, Fascicule 3 (2014): 243-250.
[4] Ghiţă, C. Mirela, Anton C. Micu, Mihai Ţălu and Ştefan Ţălu. "3D modelling of a shrink fitted concave ended cylindrical tank for automotive industry." *Acta Technica Corviniensis – Bulletin of Engineering, Hunedoara, Romania*, Tome VI, Fascicule 4 (2013): 87-92.
[5] Ghiţă, C. Mirela, Anton C. Micu, Mihai Ţălu and Ştefan Ţălu. "3D modelling of a gas tank with reversed end up covers for automotive industry.", *Annals of Faculty of Engineering Hunedoara - International Journal of Engineering, Hunedoara*, *Romania*, Tome XI, Fascicule 3 (2013): 195-200.
[6] Ghiţă, C. Mirela, Anton C. Micu, Mihai Ţălu and Ştefan Ţălu. "Shape optimization of a thoroidal methane gas tank for automotive industry." *Annals of Faculty of Engineering Hunedoara - International Journal of Engineering, Hunedoara, Romania*, Tome X, Fascicule 3 (2012): 295-297.
[7] Bică, Marin, Mihai Ţălu and Ştefan Ţălu. "Optimal shapes of the cylindrical pressurized fuel tanks." *Magazine of Hydraulics, Pneumatics, Tribology, Ecology, Sensorics, Mechatronics (HIDRAULICA)*, no. 4 (December 2017): 6-17.
[8] Ţălu, Ştefan and Mihai Ţălu. "The influence of deviation from circularity on the stress of a pressurized fuel cylindrical tank." *Magazine of Hydraulics, Pneumatics, Tribology, Ecology, Sensorics, Mechatronics (HIDRAULICA)*, no. 4 (December 2017): 34-45.
[9] Vintilă, Daniela, Mihai Ţălu and Ştefan Ţălu. "The CAD analyses of a torospheric head cover of a pressurized cylindrical fuel tank after the crash test." *Magazine of Hydraulics, Pneumatics, Tribology, Ecology, Sensorics, Mechatronics (HIDRAULICA)*, no. 4 (December 2017): 57-66.

[10] Ţălu, Mihai. "The influence of the corrosion and temperature on the Von Mises stress in the lateral cover of a pressurized fuel tank." *Magazine of Hydraulics, Pneumatics, Tribology, Ecology, Sensorics, Mechatronics (HIDRAULICA)*, no. 4 (December 2017): 89-97.
[11] Ţălu, Mihai and Ştefan Ţălu. "Analysis of temperature resistance of pressurized cylindrical fuel tanks." *Magazine of Hydraulics, Pneumatics, Tribology, Ecology, Sensorics, Mechatronics (HIDRAULICA)*, no. 1 (March 2018): 6-15.
[12] Patel, M. Pankit and Jaypalsinh Rana. "Design & optimization of LNG-CNG cylinder for optimum weight." *IJSRD - International Journal for Scientific Research & Development*, vol. 1, issue 2 (2013): 282-286.
[13] *** Certification tests of LPG and CNG. Accessed December 10, 2017. http://vzlutest.cz/en/certification-tests-of-lpg-and-cng-c3.html.
[14] Kișioglu, Yasin. "Burst tests and volume expansions of vehicle toroidal LPG fuel tanks." *Turkish J. Eng. Env.*, vol. 33 (2009): 117-125. DOI: 10.3906/muh-0905-2.
[15] Kartal, Fuat and Yasin Kișioglu. "Fatigue performance evaluations of vehicle toroidal liquefied petroleum gas fuel tanks." *J. Pressure Vessel Technol*, vol. 139, issue 4 (2017): 041402. DOI: 10.1115/1.4035976.
[16] Ţălu, Ştefan and Mihai Ţălu. "CAD generating of 3D supershapes in different coordinate systems." *Annals of Faculty of Engineering Hunedoara - International Journal of Engineering, Hunedoara, Romania*, Tome VIII, Fascicule 3 (2010): 215-219.
[17] Ţălu, Ştefan and Mihai Ţălu. "A CAD study on generating of 2D supershapes in different coordinate systems." *Annals of Faculty of Engineering Hunedoara - International Journal of Engineering, Hunedoara, Romania*, Tome VIII, Fascicule 3 (2010): 201-203.
[18] Ţălu, Ştefan. *Limbajul de programare AutoLISP. Teorie şi aplicaţii. (AutoLISP programming language. Theory and applications)*. Cluj-Napoca, Risoprint Publishing house, 2001.
[19] Ţălu, Ştefan. *Grafică tehnică asistată de calculator. (Computer assisted technical graphics)*. Cluj-Napoca, Victor Melenti Publishing house, 2001.
[20] Ţălu, Ştefan. *Reprezentări grafice asistate de calculator. (Computer assisted graphical representations).* Cluj-Napoca, Osama Publishing house, 2001.
[21] Ţălu, Ştefan. *AutoCAD 2005*. Cluj-Napoca, Risoprint Publishing house, 2005.
[22] Ţălu, Ştefan and Mihai Ţălu. *AutoCAD 2006. Proiectare tridimensională. (AutoCAD 2006. Three-dimensional designing)*. Cluj-Napoca, MEGA Publishing house, 2007.
[23] Ţălu, Ştefan. *AutoCAD 2017*. Cluj-Napoca, Napoca Star Publishing house, 2017.
[24] Țălu, Mihai. *Calculul pierderilor de presiune distribuite în conducte hidraulice. (Calculation of distributed pressure loss in hydraulic pipelines).* Craiova, Universitaria Publishing house, 2016.
[25] Ţălu, Mihai. *Mecanica fluidelor. Curgeri laminare monodimensionale. (Fluid mechanics. The monodimensional laminar flow).* Craiova, Universitaria Publishing house, 2016.
[26] Țălu, Mihai. *Pierderi de presiune hidraulică în conducte tehnice cu secțiune inelară. Calcul numeric și analiză C.F.D. (Hydraulic pressure loss in technical piping with annular section. Numerical calculation and C.F.D.)*, Craiova, Universitaria Publishing house, 2016.
[27] Ţălu, Ştefan. *Geometrie descriptivă. (Descriptive geometry)*, Cluj-Napoca, Risoprint Publishing house, 2010.
[28] Florescu-Gligore, Adrian, Magdalena Orban and Ştefan Ţălu. *Cotarea în proiectarea constructivă şi tehnologică. (Dimensioning in technological and constructive engineering graphics).* Cluj-Napoca, Lithography of The Technical University of Cluj-Napoca, 1998.
[29] Florescu-Gligore, Adrian, Ştefan Ţălu and Dan Noveanu. *Reprezentarea şi vizualizarea formelor geometrice în desenul industrial. (Representation and visualization of geometric shapes in industrial drawing).* Cluj-Napoca, U. T. Pres Publishing house, 2006.
[30] Racocea, Cristina and Ştefan Ţălu. *Reprezentarea formelor geometrice tehnice în axonometrie. (The axonometric representation of technical geometric shapes).* Cluj-Napoca, Napoca Star Publishing house, 2011.
[31] Ţălu, Ştefan and Cristina Racocea. *Reprezentări axonometrice cu aplicaţii în tehnică. (Axonometric representations with applications in technique).* Cluj-Napoca, MEGA Publishing house, 2007.
[32] Niţulescu, Theodor and Ştefan Ţălu. *Aplicaţii ale geometriei descriptive şi graficii asistate de calculator în desenul industrial. (Applications of descriptive geometry and computer aided design in engineering graphics).* Cluj-Napoca, Risoprint Publishing house, 2001.
[33] Bîrleanu, Corina and Ştefan Ţălu. *Organe de maşini. Proiectare şi reprezentare grafică asistată de calculator. (Machine elements. Designing and computer assisted graphical representations).* Cluj-Napoca, Victor Melenti Publishing house, 2001.
[34] Ţălu, Ştefan. *Micro and nanoscale characterization of three dimensional surfaces. Basics and applications*. Napoca Star Publishing House, Cluj-Napoca, Romania, 2015.
[35] *** Autodesk AutoCAD 2017 software.
[36] *** SolidWorks 2017 software.